FABRICATION AND MECHANICAL PROPERTIES OF CONTINUOUS FIBER REINFORCED ZR-BASED AMORPHOUS ALLOY COMPOSITES

Sang-Bok Lee*, Jin-Bong Kim*, Sang-Kwan Lee*
[Sang-Bok Lee#]*: leesb@kmail.kimm.re.kr
*** *Composite Materials Lab., Korea Institute of Machinery and Materials***

Abstract

In the present study, Zr-based amorphous alloy matrix composites reinforced with tungsten and stainless steel (STS) continuous fibers were fabricated without pores or defects by liquid pressing process, and their microstructures and compressive properties were investigated. The feasibility to fabricate amorphous alloy matrix composites was verified by analyses of the thermal stress and cooling behavior between matrix and metallic fibers. About 50~65 vol.% of fibers were homogeneously distributed inside the amorphous matrix, although the matrix of the STS-fiber-reinforced composite contained a small amount of crystalline phases. The compressive test results indicated that the tungsten-fiber-reinforced composite was not fractured at one time after reaching the maximum compressive strength of 2060 MPa, but showed some elongation as the compressive load was sustained by fibers. The STS-fiber-reinforced composite showed the maximum strength of about 1050 MPa, and its strength maintained over 800 MPa until reaching the strain of 40%. Both tungsten and STS fibers favorably affected the strength and ductility of the composites by interrupting the propagation of shear bands formed in the amorphous matrix, by dispersing the stress applied to the matrix, and by promoting deformation mechanisms such as fiber buckling.

1 Introduction

Unlike conventional crystalline alloys, amorphous alloys having excellent properties in strength, stiffness, wear resistance, and corrosion resistance are vulnerable to abrupt fracture due to localized shear band formation [1-6]. In order to expand the applications of amorphous alloys to functional materials as well as structural materials, thus, it is imperative to find ways to overcome the shortcomings of poor ductility and fracture toughness. To this end, active studies on developing composites in which secondary phases or reinforcements are dispersed in an amorphous alloy matrix have been conducted. Ways to fabricate amorphous alloy matrix composites include the one in which amorphous alloys are partially crystallized to disperse nanocrystallines [7], and the one in which crystalline particles are added to the amorphous melt [8]. Also included are the way to cast reinforcing fibers and amorphous alloys at the same time [9,10], and the one in which dendritic crystalline phases are generated from the amorphous melt [11].

Fabricating cast amorphous alloy matrix composites reinforced with continuous metallic fibers, it is critical to control reactions of fibers with the amorphous matrix and to develop the fabrication process technology with high reproductivity and reliability. This is because most metallic fibers except refractory metal fibers have high reactivity with the amorphous melt. To effectively fabricate amorphous alloy matrix composites reinforced with continuous fibers, it is thus necessary to introduce new-concept fabricating processes, one of which is a liquid pressing process [12,13] using low pressure near to the theoretically required minimum loading pressure. In this process, thin-plate-type composites can be readily fabricated, and the crystallization of the amorphous matrix can be prevented or minimized by rapid cooling of the melt.

In the present study, the feasibility for fabricating sound amorphous composites was predicted by investigating residual thermal stresses due to the difference in thermal expansion coefficients between amorphous matrix and continuous fibers. Tungsten and STS 304 stainless steel continuous fibers were used for reinforcements; while the former with high strength and melting point shows excellent reaction resistance to the melted matrix, the latter shows high reactivity with the melted matrix, despite its excellence in corrosion resistance and ductility. Amorphous alloy composites,

whose matrix was a Zr-based amorphous alloy, were fabricated by the liquid pressing process. Microstructures of the fabricated composites were analyzed, and their mechanical properties were evaluated by conducting compressive tests. Based on the test results, the feasibility of the liquid pressing process for fabricating the amorphous composites reinforced with continuous fibers was verified, and the possibility for extended application of amorphous alloy matrix composites to structural materials was confirmed as problems related with poor ductility and toughness were solved by compositing metallic continuous fibers onto the amorphous matrix.

2 Experimental

The Zr-based amorphous alloy used for the fabrication of amorphous alloy composites reinforced with continuous fibers was an 'LM1' alloy, which is a commercial brand name of the Liquidmetal Technologies. Its chemical composition is $Zr_{41.2}Ti_{13.8}Cu_{12.5}Ni_{10.0}Be_{22.5}$ (at.%), and it has very high amorphous forming ability, excellent hardness,

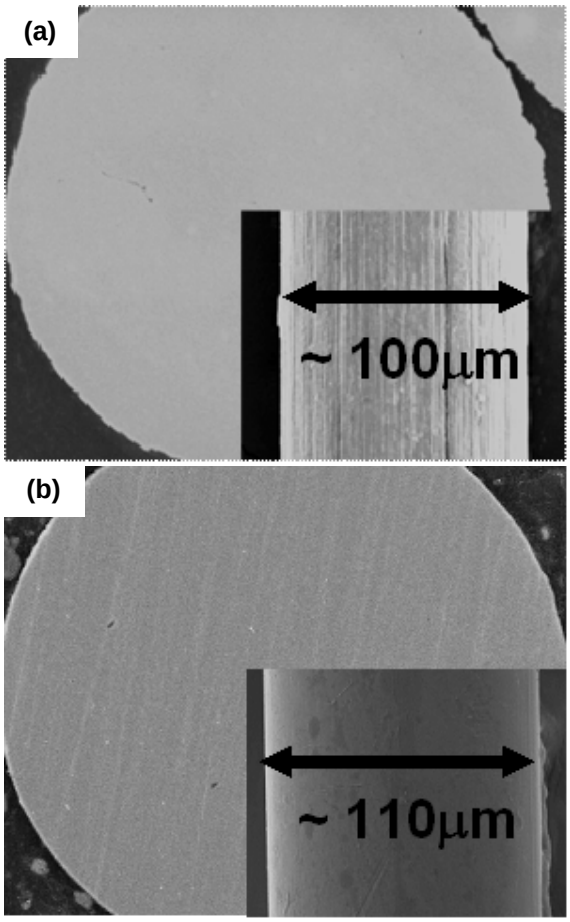

Fig. 1. SEM micrographs of (a) tungsten continuous fiber and (b) STS304 continuous fiber.

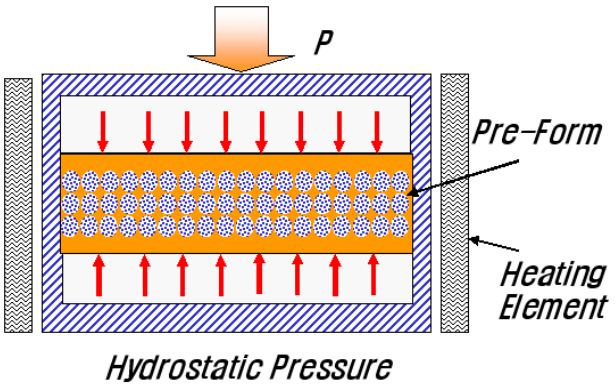

Fig. 2. Schematic diagram of the liquid pressing process used to fabricate amorphous alloy matrix composites reinforced with metallic continuous fibers.

strength, and corrosion resistance [14]. Tungsten continuous fibers having high thermal stability inside the melted matrix and STS 304 stainless steel continuous fibers having excellent strength and ductility were used as reinforcements. Scanning electron micrographs of the Zr-based amorphous master alloy and continuous fibers are presented in Figures 1. Diameters of tungsten and STS fibers are about 100 μm and 110 μm, respectively. In the amorphous master alloy, fine polygonal crystalline particles sized by 3~10 μm are distributed in the amorphous matrix. These crystalline phases are identified to be fcc phases (lattice parameter; 1.185 nm) [15], and their volume fraction is 3~4%. Representative physical properties and room-temperature tensile properties of the amorphous master alloy and continuous fibers are summarized in Table 1.

Figure 2 illustrates a schematic diagram of the liquid pressing process [16] used to fabricate amorphous alloy matrix composites. The mold interior is sized by 60×60×6 mm. A pre-form of continuous fibers and amorphous master alloy plates were inserted into the mold, degassed, and vacuumed. The mold was heated to 870oC, held for 5 minutes, and then pressed under a pressure of about 10 MPa. Pressing was accompanied with water cooling so that the solidified matrix could readily form amorphous phases.

The fabricated composites were sectioned, polished, and etched in a solution of 70 ml H2O, 25g CrO3, 20 ml HNO3, and 2 ml HF for optical and scanning electron microscope (SEM) observations. Phases formed on the composites were analyzed by X-ray diffraction (XRD). The composites were machined into cylindrical specimens of 2φ×3 mm in size, and room-temperature compression tests were

conducted on these specimens at a strain rate of 1.8×10-4 sec-1. Compressively fractured specimens were observed by an SEM after the test.

3 Results and Discussion

3.1 Solidification Behavior in Fabrication of Zr-based Amorphous Alloy Composites

In order to verify the feasibility to fabricate the amorphous alloy matrix composites by the liquid pressing process, cooling behavior of the Zr-based amorphous alloy was interpreted on the basis of the shape and size of the mold used. The software used for the calculation was the ProCAST which is a commercial solidification analysis program. The casting space of a mold with thickness of 5 mm was designed to be sized by 60×60×6 mm, which was the same size as the experimentally fabricated composites. Figure 3 shows the results predicted from the interpretation of the cooling behavior. The cooling rate of the mold region in direct contact with the coolant water is calculated to be about 500oC/s, while the rates of the side and the center regions of the composite are about 50oC/s and 10oC/s, respectively. The cooling rate of the composite is slower than that of the mold because the composite is located at the center of the mold and because the thermal conductivity of the amorphous matrix is about 1/10 of general metals. Since the slowest cooling rate at the center of the composite is much greater than the critical cooling rate (1~2oC/s) of the Zr-based amorphous alloy [17,18], the fabrication of the Zr-based amorphous composites by the liquid pressing process can be confirmed.

3.2 Thermal Stress Analysis of Composites Reinforced with Tungsten and STS Continuous Fibers

One of the structural shortcomings of the fiber-reinforced composites is the residual stress between fibers and matrix. The residual stress is attributed to the gap in thermal expansion coefficients between fibers and matrix, and the difference in temperature between glass transition temperature (360oC) of the amorphous matrix and final cooling temperature of 15oC (coolant temperature). In the present study, the residual stresses of fibers and matrix were calculated by using the finite element method. Based on the calculated results, the presence or absence of defects inside the composites was investigated. The boundary conditions were set to be infinite in the fiber

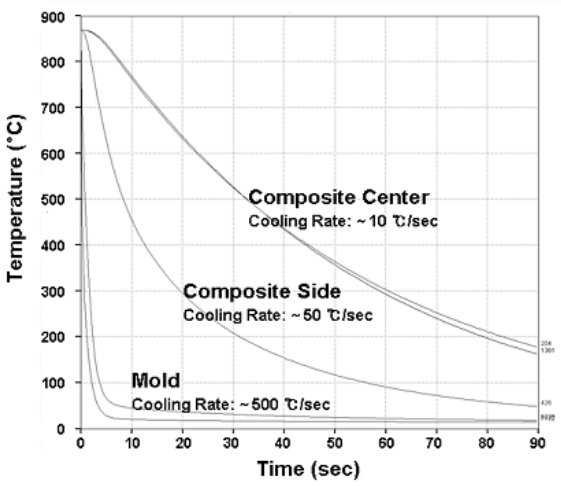

Fig. 3. Predicted cooling curves of the mold region and the side and center regions of the fabricated composite. The ProCAST (a commercial solidification analysis program) was used for the calculation.

lengthwise, while fibers (diameter; 50~55 μm, length; 500 μm) were surrounded by the amorphous matrix (radial thickness; 50~55 μm). It was assumed that material properties were irrelevant in the analyzed temperature range, and that the boundary between fibers and matrix was completely bonded.

Figures 4(a) and (b) present the residual stress state at fiber/matrix interfaces. In the tungsten-fiber-reinforced composite, as the thermal expansion coefficient of tungsten fibers is smaller than that of the matrix, the compressive stress applies in all the directions of fibers (Figure 4(a)). Because the thermal contraction of the matrix is disrupted by tungsten fibers, the compressive stress takes place in the radial direction of fibers at the fiber/matrix interface. In the hoop direction of fibers, the tensile stress starts applying, but is reduced as further away from the interface. In the longitudinal direction of fibers, the stress is tensile one, and is about the same as that in the hoop direction. It is almost constant at about 97 MPa, irrespective of the location. In the STS-fiber-reinforced composite, as the thermal expansion coefficient of STS fibers is larger than that of the matrix, the tensile stress applies in all the directions of fibers and in the radial direction of the matrix (Figure 4(b)). The compressive stress applies in the hoop direction of the matrix and in the longitudinal direction of fibers. The compressive stress in the longitudinal direction of fibers is calculated to be about 147 MPa. Since the multi-directional stresses of matrix and fibers in the tungsten- and STS-fiber-reinforced composites are much smaller than the

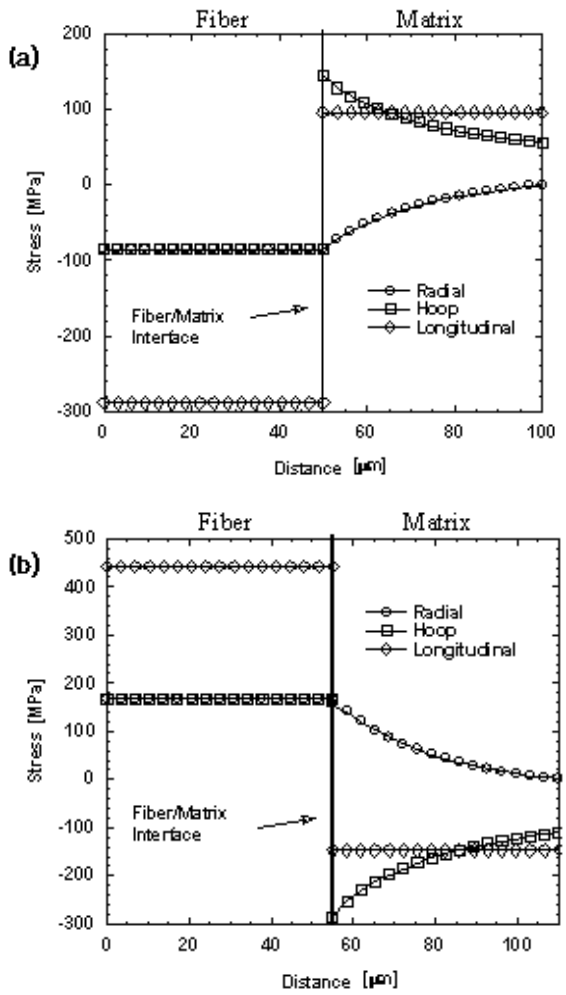

Fig. 4. Distributions of the residual stress state at fiber/matrix interfaces of the Zr-based amorphous matrix composites reinforced with (a) tungsten and (b) STS304 continuous fibers. The finite element method of a coaxial cylinder model was used for the calculation.

strengths of the matrix and fibers, it can be predicted that no defects are formed inside the composites and at the fiber/matrix interfaces.

3.3 Microstructure of Continuous-Fiber-Reinforced Composites

Figures 5(a) and (b) show X-ray diffraction patterns of the two composites reinforced with tungsten and STS fibers, respectively. Typical halo patterns of amorphous alloys and peaks of continuous fibers are observed without peaks of other crystalline phases in the both composites. This indicates that the composite matrices are mostly composed of amorphous phases.

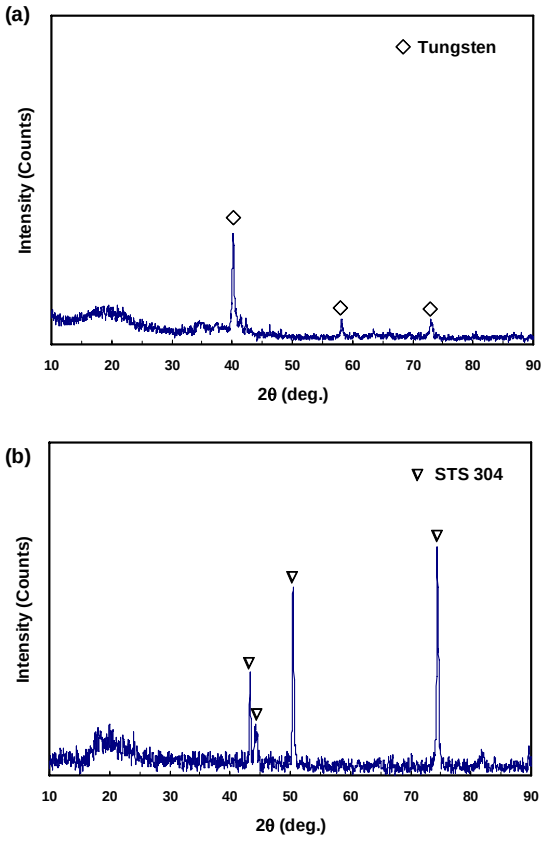

Fig. 5. X-ray diffraction patterns of the Zr-based amorphous matrix composites reinforced with (a) tungsten and (b) STS304 continuous fibers.

Figures 6(a) through (d) are SEM micrographs of the two composites. In the tungsten-fiber-reinforced composite, tungsten continuous fibers are homogeneously distributed in the matrix, and the volume fraction of fibers is about 65% as analyzed from the cross-sectional picture of the composite (Figure 6(a)). Crystalline phases are rarely observed in the amorphous matrix, and defects formed by misinfiltration or reaction products formed by interfacial reaction at fiber/matrix interfaces are hardly found (Figure 6(b)). Figures 5(a) and 6(a) and (b) show a successful fabrication of the amorphous composite reinforced with tungsten fibers by the liquid pressing process. This is because tungsten fibers with high melting point are thermally stable against the melted amorphous alloy. Since tungsten fibers are hardly diffused into the amorphous melt during the liquid pressing process, they hardly cause the composition changes of the amorphous matrix, and thus the amorphous forming ability of the Zr-based amorphous alloy can be maintained in the composite matrix. Thermal deformation which arises

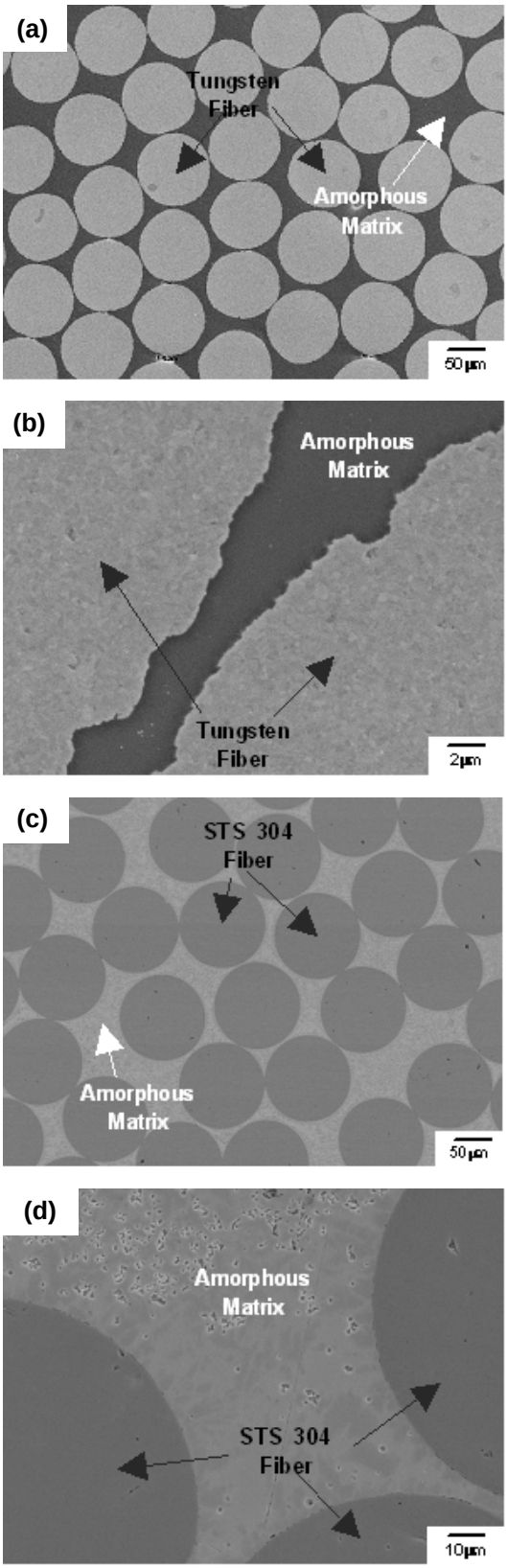

Fig. 6. SEM micrographs of the Zr-based amorphous matrix composites reinforced with (a) and (b) tungsten and (c) and (d) STS304 continuous fibers.

from the difference in thermal expansion coefficients between fibers and matrix cannot be observed as shown in Figures 6(a). This is consistent with the thermal stress analysis data of Figure 4(a).

In the STS-fiber-reinforced composite, STS continuous fibers are homogeneously distributed in the matrix, and their volume fraction is about 50% (Figure 6(c)). Pores, defects, or reaction products are not found. In the matrix, dark and bright regions, together with fine polygonal crystalline particles, are observed (Figure 6(d)). These fine polygonal crystalline particles are sized by 2~3 μm, and their volume fraction is about 7%. The dark and bright regions might be formed by the partial crystallization according to the phase separation of the amorphous melt during solidification. The bright regions indicate amorphous phases, while the dark regions show dendritic crystalline phases. The volume fraction of these dendritic crystalline phases is about 50%. According to X-ray diffraction patterns of Figure 5(b), only typical halo patterns of amorphous phases and peaks of STS fibers are observed. This might be because peaks are not visible in X-ray diffraction patterns when the volume fraction of crystalline phases is so small (less than several percentages) or when the phases are fine. As STS 304 fibers have lower melting point and less thermally stable than tungsten fibers, some elements in STS fibers are diffused when they contact with the amorphous melt of 870oC, thereby leading to the composition change of the melt. Since the amorphous forming ability is highly sensitive to alloy composition changes [19,20], the changes in the matrix composition result in the reduced amorphous forming ability and the formation of dendritic crystalline phases. When such atoms as Fe infiltrate into the matrix by diffusion, the critical cooling rate of the matrix becomes faster than the cooling rate during the composite fabrication, thereby causing the partial crystallization in the matrix. Therefore, in order to maintain the matrix as amorphous phases in the STS-fiber-reinforced composite, it is required either to use the faster cooling rate during the composite fabrication or to control the diffusion or reaction at fiber/matrix interfaces.

Though the composites fabricated by the liquid pressing process contain a small amount of crystalline phases, they do not have defects or pores formed by misinfiltration. Johnson et al [9,21,22] fabricated amorphous alloy matrix composites reinforced with continuous fibers by the gas pressure melt infiltration, and reported that 1~3 vol.% of pores were contained in the composites. These defects

seem to have been formed because the amorphous melt did not sufficiently infiltrate into the continuous fiber pre-form due to the low infiltration pressure applied to the melt. The gas pressure melt infiltration process, having relatively low infiltration pressure, might not be suitable for fabricating composites containing lots of fibers or large-scale composites reinforced with two- or three-dimensional fibers. To the contrary, as the hydrostatically applied pressure in the liquid pressing process of this study overrides the theoretical pressure required for infiltration, the amorphous melt sufficiently infiltrates into the fiber pre-form, and pores formed by the solidification contraction are eliminated. This can also be applied to the fabrication of large-scale amorphous composites reinforced with two- or three-dimensional continuous fibers as well as one-dimensional fibers.

3.4 Mechanical Properties of Continuous-Fiber-Reinforced Composites

Figures 7(a) and (b) and 8(a) and (b) show compressive stress-strain curves and SEM micrographs of the fractured compressive specimen, respectively, of the two composites. In the tungsten-fiber-reinforced composite, fracture does not take place at one time after reaching the maximum strength of 2060 MPa, but proceeds as the loading is sustained by continuous fibers (Figure 7(a)). This is one of the typical characteristics of continuous-fiber-reinforced composites [23]. In the side of the compressive specimen, some buckling is observed, and tungsten fibers are bent while sustaining the loading (Figure 8(a)). Shear bands are formed in the maximum shear stress direction in the matrix, cracks initiate, the crack propagation is interrupted by continuous fibers, fiber/matrix interfaces get separated, and the fracture proceeds. In the STS-fiber-reinforced composite, the maximum strength is 1050 MPa, which is lower than that of the tungsten-fiber-reinforced composite (Figure 7(b)). Fracture does not take place until reaching the strain of about 40%, while keeping the strength over 800 MPa. As in typical amorphous alloys, the compressively fractured specimen shows the progression of fracture at the maximum shear stress direction (about 45° angle against the compressive loading direction) (Figure 8(b)). Figure 9 shows an SEM micrograph of the cross-sectional area of the compressively fractured specimen of the STS-fiber-reinforced composite. Many cracks initiate in the matrix around the main shear crack propagated at 45° angle against the loading direction, and STS fibers are bent and

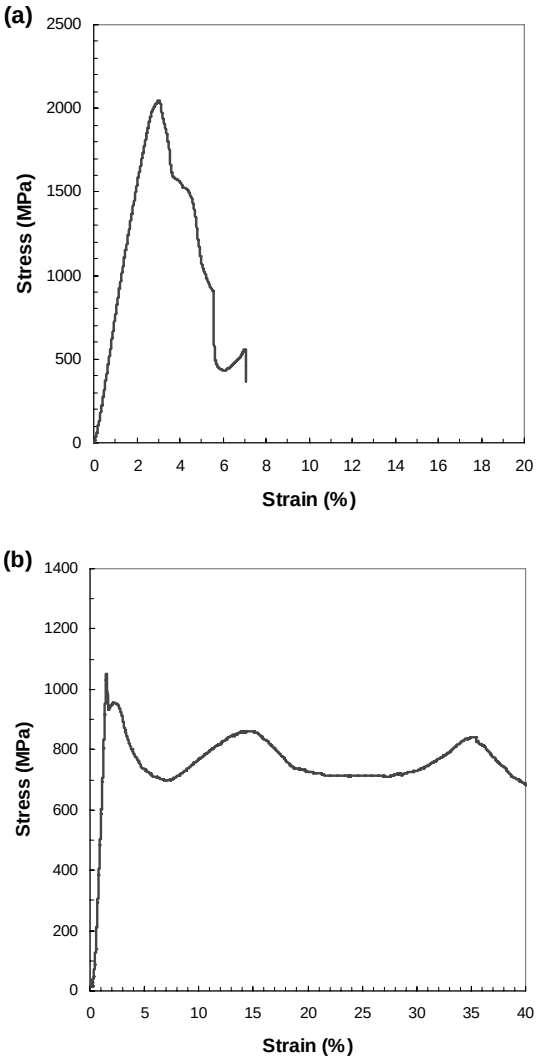

Fig. 7. Compressive stress-strain curves of the Zr-based amorphous matrix composites reinforced with (a) tungsten and (b) STS 304 continuous fibers.

unfractured. According to this deformation of STS fibers, the STS-fiber-reinforced composite shows the large ductility, while maintaining the strength over a certain level.

Reasons behind the higher maximum compressive strength of the tungsten-fiber-reinforced composite (2060 MPa) than that of the amorphous master alloy (1920 MPa) include: (1) Tungsten fibers have higher strength than the amorphous master alloy (Table I), and (2) the residual tensile stress of about 100 MPa present in the matrix along the longitudinal direction of fibers plays a buffering role of the compressive stress during the compression test (Figure 4(a)). In the STS-fiber-reinforced composite, the maximum compressive strength is 1050 MPa, which is still lower than the 1300 MPa expected from

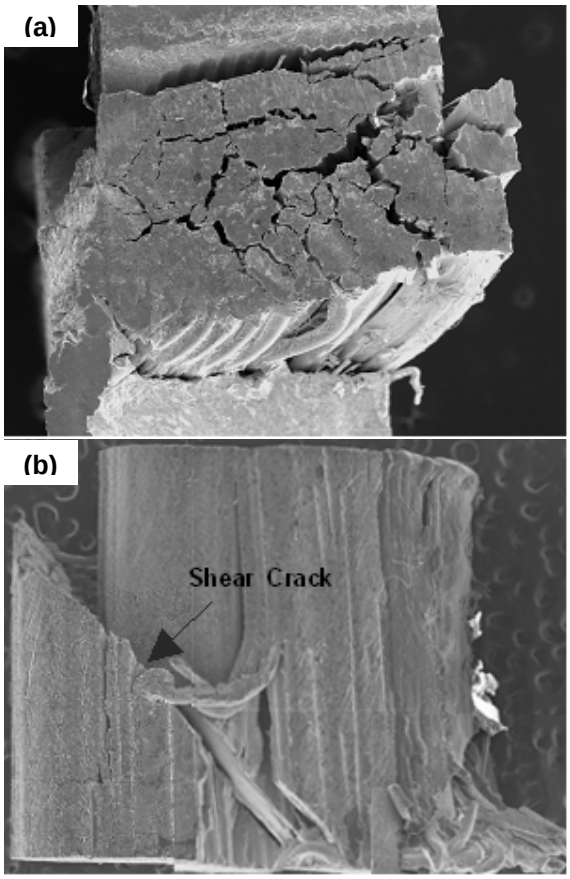

Fig. 8. SEM fractographs of the Zr-based amorphous matrix composites reinforced with (a) tungsten and (b) STS 304 continuous fibers.

the rule of mixtures, despite considering that the maximum strength of STS fibers is lower by 1/3 than that of the amorphous master alloy. This is associated with the presence of the residual compressive stress of about 150 MPa in the matrix along the longitudinal direction of fibers. This residual compressive stress works for additional compressive loading during the compressive test and for initiating the fracture at the lower strength than the matrix's maximum strength. These results indicate that the residual thermal stresses formed in the cast composites significantly affect mechanical properties of the composites, and that the thermal stress analysis data of this study should be seriously considered when fabricating the cast composites.

In general, amorphous alloys hardly show any plastic regions at room temperature under tensile and compressive loading conditions as the plastic deformation is concentrated on localized shear bands [6,24,25]. The localized plastic deformation at one shear band is very large, and only a few shear bands work to cause a brittle fracture. However, in the

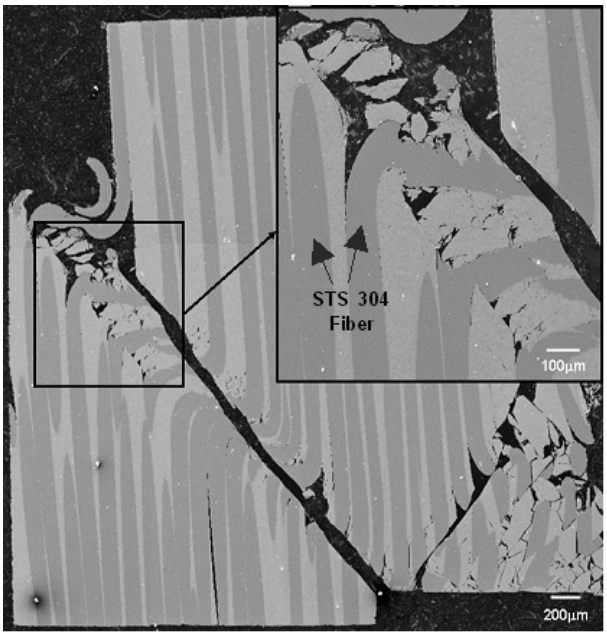

Fig. 9. Cross-sectional SEM micrographs of the Zr-based amorphous matrix composite reinforced with STS 304 continuous fibers.

composites fabricated in the present study, metallic continuous fibers interrupt the propagation of shear bands formed in the amorphous matrix, disperse the stress applied to the matrix, and promote deformation mechanisms such as fiber buckling, thereby favorably affecting the strength and ductility of the composites. Particularly in the STS-fiber-reinforced composite, the ductility is greatly enhanced as STS fibers are sufficiently plastically deformed.

The present results in which amorphous alloy matrix composites reinforced with metallic continuous fibers were fabricated by the liquid pressing process not only help better understanding of the formation process of microstructures, but also confirm the possibility to eventually overcome shortcomings of low ductility while maintaining advantages of amorphous alloys. When amorphous alloys are reinforced with metallic continuous fibers by the liquid pressing process, composites with excellent interfacial bonding between matrix and fibers can be successfully fabricated without pores or defects. The tungsten-fiber-reinforced composite shows an increase in the compressive strength and ductility over the amorphous alloy, while the STS-fiber-reinforced composite shows a dramatic enhancement in ductility up to 40% despite some reduction in strength. Because of the excellence of these composites in high strength, ductility, and

fracture toughness, new possibilities are open to be applied to structural materials requiring excellent properties. In order to make further improvements in microstructures and properties of the amorphous alloy matrix composites, continuous studies are required to select and develop new fibers and matrix alloys, to establish liquid pressing process parameters, and to elucidate mechanisms involved in improving strength, ductility, and fracture toughness.

4 Conclusions

In this study, Zr-based amorphous alloy matrix composites reinforced with metallic continuous fibers were fabricated by the liquid pressing process, and their microstructures and compressive properties were investigated to reach following conclusions.

1) The feasibility to fabricate amorphous alloy matrix composites without forming pores or defects due to thermal deformation was verified in this study, based on the analyses of the thermal stress and cooling behavior between matrix and metallic fibers.

2) Using the liquid pressing process, Zr-based amorphous alloy matrix composites reinforced with metallic continuous fibers were successfully fabricated without pores or defects, and showed excellent fiber/matrix interfaces. About 65 vol.% of tungsten fibers were homogeneously distributed inside the amorphous matrix in the tungsten-fiber-reinforced composite. In the STS-fiber-reinforced composite, about 50 vol.% of STS fibers were distributed in the amorphous matrix containing a small amount of crystalline phases.

3) According to the compressive test results, the tungsten-fiber-reinforced composite was not fractured at one time after reaching the maximum compressive strength of 2060 MPa, but showed some elongation as the compressive load was sustained by tungsten fibers. The STS-fiber-reinforced composite showed the maximum strength of about 1050 MPa, and its strength maintained over 800 MPa until reaching the strain of 40%.

4) Both tungsten and STS fibers favorably affected the strength and ductility of the composites by interrupting the propagation of shear bands formed in the amorphous matrix, by dispersing the stress applied to the matrix, and by promoting deformation mechanisms such as fiber buckling. These findings confirmed the possibility to apply them to structural materials requiring excellent properties.

Acknowledgement

This work was performed as a part of basic research project (Development of metallic fiber reinforced amorphous alloy composites) of KIMM and supported by MOST in Korea.

References

[1] R.D. Conner, R.B. Dandliker, and W.L. Johnson: Acta Mater., 1998, vol. 46, pp. 6089-102.

[2] A. Inoue: Acta Mater., 2000, vol. 48, pp. 279-306.

[3] Z.F. Zhang, J. Eckert, and L. Schultz: Acta Mater., 2003, vol. 51, pp. 1167-79.

[4] K.M. Flores and R.H. Dauskardt: Acta Mater., 2001, vol. 49, pp. 2527-37.

[5] J.C. Lee, Y.C. Kim, J.P. Ahn, and H.S. Kim: Acta Mater., 2005, vol. 53, pp. 129-39.

[6] J.G. Lee, D-G. Lee, S. Lee. N.J. Kim: Metall. Mater. Trans. A, 2004, vol. 35A, pp. 3753-61.

[7] C. Fan, C. Li, A. Inoue, and V. Haas: Phys. Rev. B, 2000, vol. 61B, pp. R3761-63.

[8] H. Choi-Yim, R. Busch, U. Koster, and W.L. Johnson: Acta Mater., 1999, vol. 47, pp. 2455-62.

[9] R.B. Dandliker, R.D. Conner, and W.L. Johnson: J. Mater. Res., 1998, vol. 13, pp. 2896-901.

[10] P. Wadhwa, J. Heinrich, and R. Busch: Scripta Mater., 2007, vol. 56, pp. 73-76.

[11] L.-Q. Xing, Y. Li, K.T. Ramesh, J. Li, and T.C. Hufnagel: Phy. Rev. B, 2001, vol. 64B, pp. 180201-04.

[12] Y.H. Jang, S.S. Kim, S.K. Lee, D.H. Kim, and M.K. Um: Compo. Sci. Tech., 2005, vol. 65, pp. 781-84.

[13] S.B. Lee, K. Matsunaga, Y. Ikuhara, and S.K. Lee: Mater. Sci. Eng. A, 2007, vol. 449-451A, pp. 778-81.

[14] A. Peker and W.L. Johnson: Appl. Phys. Lett., 1993, vol. 63, pp. 2342-44.

[15] J.G. Lee, D.G. Lee, S. Lee. K.M. Cho, I.M. Park, and N.J. Kim: Mater. Sci. Eng. A, 2005, vol. 390A, pp. 427-36.

[16] Y.H. Jang, S.S. Kim, Y.C. Jung, and S.K. Lee: J. Kor. Inst. Met. & Mater., 2004, vol. 42, pp. 425-31.

[17] Y.J. Kim, R. Busch, W.L. Johnson, A.J. Rulison, and W.K. Rhim: Appl. Phys. Lett., 1996, vol. 68, pp. 1057-59.

[18] S.B. Lee and N.J. Kim: Mater. Sci. Eng. A, 2005, vol. 404A, pp. 153-58.

[19] Y. Zhang, D.Q. Zhao, M.X. Pan, and W.H. Wang: J. Non-cryst. Solids, 2003, vol. 315, pp. 206-10.

[20] X.F. Zhang, Y.M. Wang, J.B. Qiang, Q. Wang, D.H. Wang, D.J. Le, C.H. Shek, and C. Dong: Intermetallics, 2004, vol. 12, pp. 1275-78.

[21] R.D. Conner, R.B. Dandliker, V. Scruggs, and W.L. Johnson: Int. J. Impact Eng., 2000, vol. 24, pp. 435-44.

[22] H. Choi-Yim, R.D. Conner, F. Szuecs, and W.L. Johnson: Acta Mater., 2002, vol. 50, pp. 2737-45.

[23] R. Vaidya and K.N. Subramanian: SAMPE J., 1993, vol. 29, pp. 26-30.

[24] C.J. Gilbert, R.O. Ritchie, and W.L. Johnson: Appl. Phys. Lett., 1997, vol. 71, pp. 476-78.

[25] K. Kawamura, H. Kato, A. Inoue, and T. Masumoto: Appl. Phys. Lett., 1995, vol. 67, pp. 2008-10.

Table 1. Physical and tensile test properties of tungsten and STS 304 continuous fibers and Zr-based amorphous alloy.

Material	Fiber Diameter (㎛)	Density (g/cm^3)	Melting Temp. (^oC)	Thermal Expansion Coefficient ($10^{-6}/^oC$)	Elastic Modulus (GPa)	Yield Strength (MPa)	Ultimate Strength (MPa)	Elongation (%)
Tungsten Continuous Fiber	~ 100	19.3	3370	4.6	411	1700	2350	~ 1.5
STS 304 Continuous Fiber	~ 110	7.9	1455	17.3	190	380	687	~ 12
Zr-Based Amorphous Alloy		6.1	720	8.5	96	1920	1920	~ 2